On-Wafer Penetration Depth Measurements of Superconducting Films

Michael E. Cyberey*, Robert M. Weikle and Arthur W. Lichtenberger
University of Virginia Microfabrication Laboratories, VA, USA
*Contact: mc8qr@virginia.edu

***Abstract*— An on-wafer measurement technique allowing measurement of a superconducting film's penetration depth without post device-fabrication separation of the chips has been investigated. Coplanar waveguide (CPW) probes and a CPW to microstrip transition are utilized, allowing the use of commercially available LakeShore® CPX-1.5K cryogenic CPW probing station capable of microwave measurements to 50 GHz. The use of CPW probes allows for rapid prototyping and is nondestructive to the device wafers, and hence compatible with many device fabrication technologies. Measurement techniques utilizing resonant microwave circuits have been reported [1],[2], but require mounting to custom-made test fixtures and are not performed on-wafer, but instead on individual diced devices. However, such a dicing requirement is incompatible with our ultra-thin Si, Au beam-lead chip architecture [3]. In addition to a traditional resonant circuit measurement technique, a technique that uses on-wafer calibration standards is discussed. The on-wafer calibration eliminates possible effects introduced by the testing setup and potentially offers additional advantages such as a size reduction and a direct measurement of RF loss. The designs and results for both measurement techniques are reported for NbTiN films.**

I. Introduction

Superconducting circuits have found broad application in THz electronics, with energy gap materials allowing operation at higher frequencies. Precise knowledge of the films' magnetic penetration depth is useful in the optimization of material quality and integral to RF circuit design.

With regard to the material quality of sputtered films, there are multiple variables which may require optimization. For larger energy gap superconductors, such as NbN and NbTiN, normal-state resistivity, stress, and transition temperature have been used as figures of merit for optimization [4],[5]. Using BCS theory, the penetration depth of a film can be approximated from these measurements using the relation [4]

$$\lambda_l(nm) \approx 105\left[\frac{\rho(\mu\Omega - cm)}{T_c(K)}\right]^{(\frac{1}{2})} \qquad (1)$$

where λ_l is the London penetration depth, ρ is the normal-state resistivity, and T_c is the transition temperature. A direct measurement of penetration depth can therefore also be used as a figure of merit. Having test structure designs compatible with normal device fabrication processes will alleviate the need to require separate material test wafers.

The use of resonant circuits though the microstrip resonator technique is a proven method for the measurement of the penetration depth of thin films [1]. One typical drawback is the necessity to dice devices and mount them in a custom fixture. This requirement limits the usability when fabrication techniques require thinning of the whole wafer. In an attempt to address this limitation, new resonators based on those published by Lea [2] are designed and adapted for use with a cryogenic CPW probing station. The use of such a system ensures testing can be performed on-wafer and non-destructively.

Although this method can be adapted to cryogenic probing, it still has fundamental limitations in terms of size requirements. The method relies on measuring the resonant frequencies which only occur at multiples of half wavelengths of the fundamental resonance. As such, transmission lines must be wavelengths in length, consuming valuable area on actual device-containing wafers. As the wavelengths decrease with increasing measurement frequency, a trade-off between the decrease in required resonator length and increased system losses at high measurement frequency occurs. Through the use of a CPW probing station, the resonators have been tested up to 50 GHz to show the upper limit of the practical measurement frequency using our probe station.

To further reduce the required physical size of test structures, a method of determining the penetration depth without the need for long transmission lines is investigated. Through the use of on-wafer TRL standards, the phase velocity can be directly determined from the phase of the de-embedded S-parameters. Since the phase velocity is determined from S-parameters across all and not only certain resonant frequencies, the need to fabricate lines of multiple wavelengths is removed. An on-wafer set of TRL standards was designed and fabricated. The TRL standards set a reference plane after a CPW to microstrip transition. In theory, when such a calibration is implemented the phase velocity can be determined solely from the calibration standards and no additional devices.

II. Experimental Methods and Design

A. Penetration Depth Calculations

The impedance of a superconducting microstrip line differs from that of an ideal lossless line of zero resistance. The penetration depth affects the impedance of the superconducting microstrip line through the change in kinetic inductance introduced by cooper pairs. The solutions for the inductance and capacitance of a superconducting microstrip line have been published by W.H. Chang [6] as

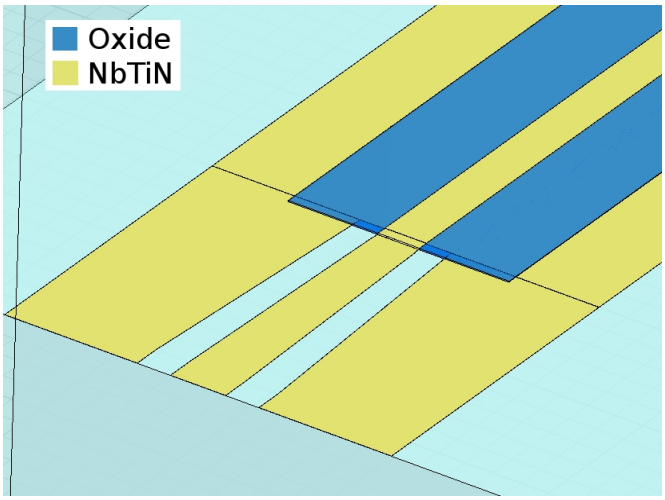

Fig. 1 A screenshot from HFSS® showing a portion of the 3D model before design simulations. The CPW line is shown as well as the abrupt transition to microstrip. The device is symmetric about the center of the microstrip line.

$$L = \frac{\mu_0}{W K}\left[h + \lambda_1 \left(\coth\left(\frac{t_1}{\lambda_1}\right) \ldots \right.\right. \\ \left.\left. \ldots + \frac{2\,p^{1/2}}{r_b} csch\left(\frac{t_1}{\lambda_1}\right) \right) + \lambda_2 \coth\left(\frac{t_2}{\lambda_2}\right) \right] \quad (2)$$

and

$$C = \frac{\epsilon \epsilon_0 W}{h} K \quad (3)$$

where W is the center conductor line width, h is dielectric thickness, t_1, λ_1 and t_2, λ_2 are the thickness and the penetration depth of the center conductor and ground plane respectively. The factors K, r_b and p take into account fringing fields and are determined by the microstrip geometries. These factors are included in Chang's paper [6].

Noting that only the inductance per unit length is a function of penetration depth and that for our design both metal layers are the same, $\lambda_1=\lambda_2=\lambda_l$; the phase velocity is simply

$$v_p = \frac{1}{\sqrt{(L(\lambda_l)C)}} \quad (4)$$

Once phase velocity of a microstrip line is measured, Matlab® is used to solve Eqs. 2-4 for the penetration depth.

B. Resonator Device Design

The design of the first device relies on the microstrip resonator technique to determine phase velocity and calculate the penetration depth. The details of the resonance measurement technique have been covered in detail by Langley [1] and Lea [2]. Our design consists of a low impedance ~1 Ω microstrip line connected at both ends by a 50 Ω CPW line designed to be probed by a 150 µm pitch 50 Ω CPW probe. The impedance mismatch at the abrupt CPW to microstrip transition introduces the reflections necessary to measure distinctive resonant frequencies. Fig 1 displays the design including the abrupt CPW to microstrip transition. Multiple lengths of line ranging from 5 mm to 3.5 cm have been included in the design.

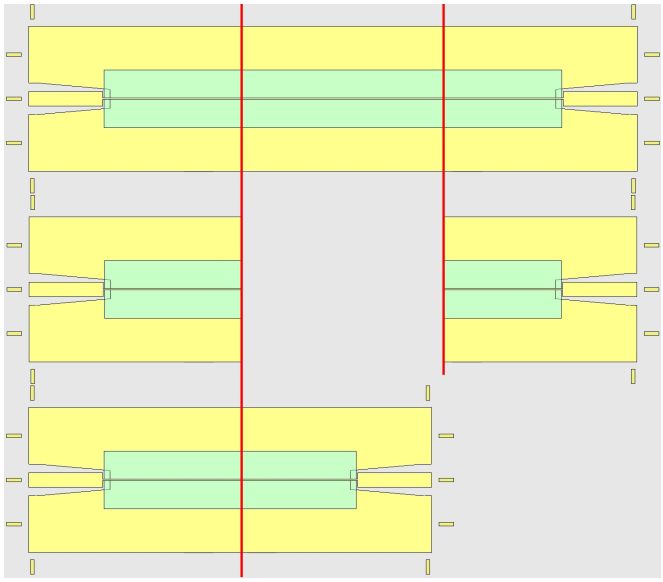

Fig. 2 The Line, Reflect, and Through standards from top to bottom, respectively. All standards contain alignment keys to aid with repeatable placement of CPW probes. The reference planes are displayed as the solid vertical lines.

C. TRL Calibration / Direct Phase Measurement

The phase velocity of a transmission line of know length is simply

$$v_p = \frac{\omega l}{\theta} \quad (5)$$

Where ω is the angular frequency, θ is the phase difference across the line, and and l is the length of the line. If the measurement system can be de-embedded, phase can be directly measured. Once the phase velocity is determined using Eq. 5, penetration depth can be calculated from Eqs. 2-4. Since a CPW probe is used and a CPW to microstrip transition is to be employed, an on-wafer calibration is required to de-embed the probes and transition.

A set of on-wafer TRL standards was designed and fabricated. The standards set a reference plane for phase measurement after the CPW to microstrip transition. Fig 2 displays the calibration standards and outlines the location of the reference plane. The standards utilize a zero-length through, a 90° line at the center frequency, and a zero-length short for the reflect. The short is created by physically connecting the center-conductor of the microstrip line to the ground plane though a hole defined in the dielectric layer. Through the use of the NIST StatistiCAL® algorithm [9], the measured response of the standards is used to de-embed the entire measurement system before this reference plane.

Unlike the previous resonator design where high reflections are desirable, the design of the CPW to microstrip transition is such to allow minimal reflections to enable maximum power transmission across the entire frequency band. To reduce reflections, a smaller microstrip line width

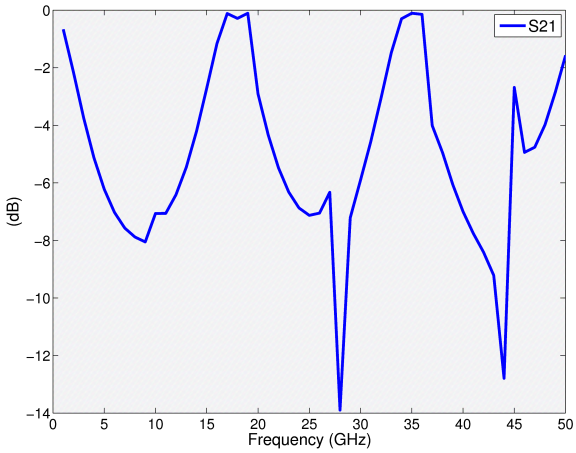

Fig. 3 HFSS simulation results for the CPW to microstrip transition are shown above. S_{21} is shown from 1 to 50 GHz and less then 8 dB attenuation is seen through most of the band.

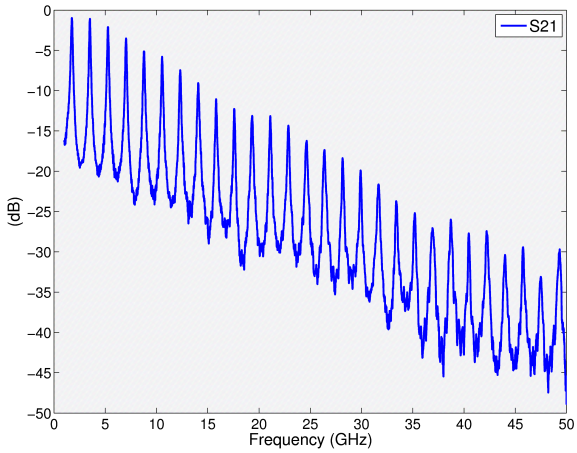

Fig. 4 The clear resonant peaks of S_{21} are seen from 1 to 50 GHz.

is employed to increase the impedance. The CPW line is also tapered to gradually reduce the 50 Ω input impedance at the probing location and provide a better match at the transition. The design was simulated using HFSS® to verify minimal reflections and a transmission coefficient with less than -10 dB attenuation. The superconductivity of the thin films was taken into account by noting the surface impedance of a superconducting film of thickness t is

$$Z_s = (j\omega\mu_0\lambda_l)\frac{e^{\frac{t}{\lambda_l}} + \frac{Z_n - j\omega\mu_0\lambda_l}{Z_n + j\omega\mu_0\lambda_l}e^{\frac{-t}{\lambda_l}}}{e^{\frac{t}{\lambda_l}} - \frac{Z_n - j\omega\mu_0\lambda_l}{Z_n + j\omega\mu_0\lambda_l}e^{\frac{-t}{\lambda_l}}} \approx j\omega\mu_0\lambda_l \coth\left(\frac{t}{\lambda_l}\right) \quad (6)$$

where Z_n is the impedance of free space and $Z_n >> j\omega\mu_0\lambda_l$ [7]. Using this approximation, surface impedance boundaries for the films were set in HFSS. Fig 3 shows the results of the simulation, a transmission coefficient of >-8 dB is seen across the majority the band from 1-50 GHz. In addition to the calibration standards, additional lines of 1-3 cm in length were included for comparison.

D. Equipment

All aspects of fabrication were performed in the University of Virginia Microfabrication Laboratories. The designs were directly exported from HFSS to CAD format and were transferred to chrome plated photo-masks using a Heidelberg DWL 66 Laser Mask Writer.

DSP silicon wafers (50 mm diameter with 1500 Å thermal oxide) were chosen as the carrier substrate. The NbTiN films were deposited by reactive sputtering of NbTi through an Ar/N_2 plasma. The details of the NbTiN deposition and system used are previously covered in detail [5]. The oxide layers were deposited by RF diode sputtering of a 5 in quartz target. The substrate was mounted using high vacuum grease to a water-cooled grounded platter with a target-substrate separation of 1.5 in.

Film stress was measured by use of an optical profilometer which measures the change in wafer curvature after a deposition is completed. Film resistivity was recorded using the four point probe technique. All film thicknesses were measured using a Dektak® 8 stylus profiler. Dielectric constant of the oxide was determined by measuring the capacitance of multiple capacitors fabricated on-wafer alongside devices. The capacitance was measured using a Wayne Kerr LCR meter connected to the DC probes of the CPX cryostat.

The RF measurements were performed in a LakeShore CPX 1.5K Flow Cryostat equipped with two Picoprobe® CPW microwave probes. All S-parameters were measured and recorded using mwavepy [8] and an HP8510C VNA. A full two port first tier calibration was performed before connecting the VNA to the cryostat. Raw first tier calibrated data was recorded and the subsequent TRL calibration was applied as a second tier calibration using the NIST StatistiCAL calibration package. Temperatures were monitored using a LakeShore Model 340 Temperature Controller and a DT-670 temperature sensor located on the cryostat's stage. Apiezon N® grease was used as a thermal interface material between the substrate and stage.

We found that during the time of testing, the cryostat was equipped with one incorrect model probe. Testing was possible using this probe, but as a result of probe geometries, repeatable and reliable contact was difficult to achieve. This has little effect on uncalibrated resonator measurements but can play a critical role in the accuracy of the calibrated device measurements.

III. Results

A. Resonator Measurements

Five resonators with lengths ranging from 5 mm to 3.5 cm were tested. A sweep from 1 to 50 GHz using 8001 data points was recorded. Noting the limitation of the HP8510C to record a maximum of 801 data points, this was achieved by breaking the sweep into smaller bands and stitching

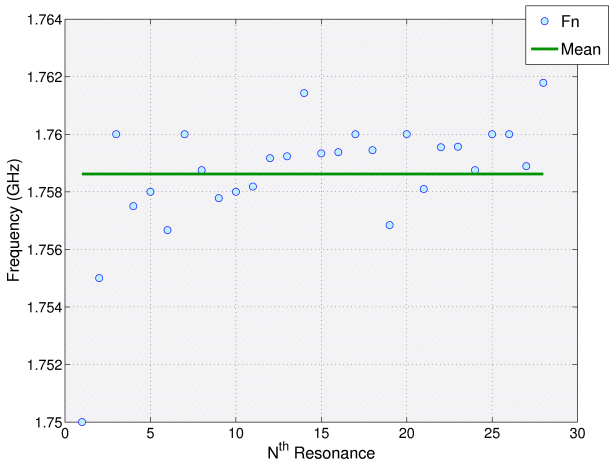

Fig. 5 The fundamental resonances, F_n, and their mean plotted across the N^{th} order resonance from which they were determined. The standard deviation is 2.2 MHz and the RMS error is 0.12%.

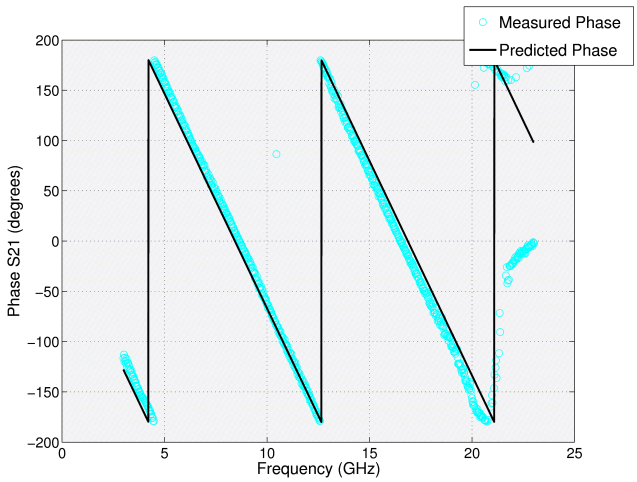

Fig. 6 The measured phase plotted alongside the phase predicted using the calculated penetration depth from the resonator measurements. Agreement is seen across the band until around 20 GHz, where it is believed the TRL calibration reaches the upper limit of it's bandwidth.

together 10 separate scans. Fig 4 shows the resulting S_{21} measurements and the sharp resonant peaks of the 3.5 cm long resonator. The fundamental resonances were determined at each peak by dividing the frequency of the n^{th} peak by n. This method was chosen over simply measuring the difference in peak locations in order to reduce measurement error. If we model the measured frequency, f_{meas}, as the actual frequency, f, plus an uncertainty term, e, the fundamental frequency, f_{meas}/n, has the uncertainty reduced by a factor of n.

$$\frac{f_{meas}}{n} = \frac{(f+e)}{n} = \left(\frac{f}{n}\right) + \left(\frac{e}{n}\right) \qquad (7)$$

Fig 5 shows the measured fundamental resonances, as well as their mean, plotted across the n^{th} order. The standard deviation to the mean is only 2.2 MHz. This reduction in the uncertainty leads to a standard deviation which is less than the frequency spacing, 6.1 MHz, of the scan. The RMS error of the fundamental resonance is a remarkably low 0.12%.

Using the results of the 5 resonators, an average penetration depth of 281 nm with a standard deviation of only 2.9 nm was calculated. Using the NbTiN film's measured resistivity of 107 μΩ-cm and measured transition temperature of 14.45 K, BCS theory (Eq. 1) predicts a penetration depth of 285 nm, in good agreement with the measured values.

B. TRL Measurements

TRL measurements were recorded over a range of 3-23 GHz, which is the designed bandwidth of the single line TRL calibration. All TRL calibration standards were measured as well as lines of varying length. The calculated penetration depth of 281 nm, from the previous resonator measurements, was used to predict the calibrated response. The response was then compared with this theoretical prediction to first give qualitative evidence the calibration is working correctly. Fig 6 shows this agreement and one can see that around 20 GHz, the calibration begins to fail. TRL calibrations are only valid within a limited bandwidth, determined by the length of the line standard, and this is near the upper limit. For this reason, only data below 20 GHz was used for the penetration depth calculations. For the quantitative results, the calibrated results were used to solve for the phase velocity as shown in Eq. 5. Three of the five measured lines gave usable results and a penetration depth of 284 nm with a standard deviation of 9.5 nm was calculated.

IV. Conclusions and Future Work

Two methods of measuring penetration depth have been investigated. Through the use of CPW probes and a cryogenic probing station, both methods introduce a method of non-destructively measuring penetration depth on-wafer. A notable benefit of using CPW probes is the ability to rapidly test multiple devices. Previous methods through the use of dip-sticks and dicing of individual devices can take hours to test a single device. Another benefit is that the on-wafer devices can be incorporated to any mask set that includes at least two superconducting layers and one oxide layer. Both test structures can also be fabricated on the same wafer and tested side-by-side in the same testing setup.

The CPW-adapted resonator measurement has been shown to provide results which agree well with each other, as well as BCS theory. This method provides accurate on-wafer penetration depth measurements and has shown consistency up to 50 GHz.

The phase measurement devices produced results for penetration depth that agreed well with both the resonator measurements and BCS theory. When directly compared to the resonator measurements, they did have a standard deviation nearly 3 times larger and only 3 of the 5 tested devices showed usable results. With regard to these disparities, it should be noted that during the time of testing, an incorrect model probe had been provided by LakeShore and had to be used. The physical difference of the incorrect model resulted in difficultly with repeatable probe placement. Such repeatable placement is an integral part of any calibration scheme.

The motivation of pursuing calibrated measurements can be seen in the simplicity of Eq. 5. Phase velocity, and hence penetration depth, can be extracted from the TRL standards themselves with no additional devices. The calibrated phase information of the line standard can be used to determine the phase velocity when such a calibration is perfected. The line standard for TRL calibrations is generally only a quarter-wavelength at center frequency, a much shorter length when compared to the multiple-wavelength long lines required for resonance measurements. An additional benefit is that penetration depth results can be obtained from any wafer where TRL standards are already present, such is the case for many wafers containing superconducting microwave circuits.

For future work, accurate resonance measurements at frequencies up to 50 GHz will allow the testing of resonator devices of reduced size. Further work and improvements will be made to the probe station in efforts to increase the accuracy of TRL calibrations. The TRL calibration will be retested, including additional calibration standards designed for higher frequencies. It is also believed RF loss can be seen in the magnitude of the transmission coefficient of a transmission line inserted between our two reference planes. This idea will also be tested in future work.

Acknowledgment

The authors thank Alex Arsenovic for his helpful critiques, Theodore Reck for his help in photo-mask fabrication, and J. M. Beatrice for his work as UVML Facility Manager.

References

[1] B. W. Langley, S. M. Anlage, R. F. W. Pease, and M. R. Beasley, "Magnetic penetration depth measurements of superconducting thin films by a microstrip resonator technique," *Review of scientific instruments.* , vol. 62, pp. 1801-1812, July 1991

[2] Lea, Dallas Millard, Jr., "Integrated test structures for characterization of thin films for superconductor-insulator-superconductor devices and circuits," PhD Dissertation, University of Virginia, 1996

[3] R.B. Bass *et. all*, "Ultra-Thin Silicon Chips for Submillimeter-Wave Applications ," in *ISSTT'04*, 2004, paper 10.3, pp. 392

[4] T. Matsunaga, H. Maezawa, and T. Noguchi, "Characterization of NbTiN Thin Films Prepared by Reactive DC-Magnetron Sputtering ," *IEEE transactions on applied superconductivity.* , vol.13, NO. 2, pp. 3284-3287, June 2003

[5] T. W. Cecil, M. E. Cyberey, R. E. Matthews, J. Z., and A.. W. Lichtenberger, "Development of Nb/Al-AlN/NbTiN SIS Junctions With ICP Nitridation," *IEEE transactions on applied superconductivity.* , vol.19, NO. 3, pp. 409-412, June 2009

[6] W. H., Chang, "The inductance of a superconducting strip transmission line," *Journal of applied physics* , vol. 50, issue. 12, pp. 8129-8134, Dec. 1979

[7] A. R. Kerr, "Surface Impedance of Superconducting and Normal Conductors in EM Simulators," *MMA Memo.* No. 245 Jan. 1999

[8] (2010) mwavepy – Project Hosting. [Online]. Available: http://code.google.com/p/mwavepy/

[9] D. F. Williams, J. C. M. Wang, and U. Arz, Member, "An Optimal Vector-Network-Analyzer Calibration Algorithm," *IEEE transactions on microwave theory and techniques*, vol. 51, NO. 12, Dec. 2003